Emulsion Layer Model for Wall Heat Transfer in a Circulating Fluidized Bed

M. Mahalingam and Ajit Kumar Kolar
Heat Transfer and Thermal Power Lab., Dept. of Mechanical Engineering, Indian Institute of Technology, Madras 600 036, India

An emulsion layer model is presented which predicts the thickness of a downward-moving emulsion layer along the wall of a circulating fluidized bed, the mean solids velocity, and the solids flux in the layer. Also presented is a heat transfer model which, in combination with the emulsion layer model, predicts the low-temperature data very well. An alternate slab model proposed for the radiative component in a high-temperature circulating fluidized bed agrees well with experimental data. The heat transfer predictions of the overall model for such operating parameters as solid circulation flux, suspension temperature, length of the heat transfer surface, superficial gas velocity, and mean particle size are in good agreement with the published data for long surfaces.

Introduction

Interest in circulating fluidized bed (CFB) boilers has been growing ever since this technology was successfully adopted for the efficient combustion of low-grade fuels in an environmentally acceptable manner. However, theoretical understanding of several fundamental aspects of CFB technology is far from satisfactory. Heat transfer is one such area that needs further investigations.

Heat extraction in a circulating fluidized bed can be accomplished through any one (or a combination) of the following heat absorption surfaces:

- Tubular surfaces suspended from the top near the CFB riser exit
- Vertical membrane wall surfaces that form part of the CFB riser walls
- Heat exchanger bundles immersed in an external bubbling fluidized-bed heat exchanger.

Of these three, the membrane wall surfaces appear to be preferred in practice. The correct sizing of these membrane wall surfaces is very important to ensure proper operation, load turndown, and system optimization of the CFB boilers. It is, therefore, essential to thoroughly understand the mechanisms of heat transfer between the gas-solid suspension in the CFB and the membrane wall surface, and to develop an appropriate model to predict the heat transfer. This demands a clear understanding of the structure and the dynamics of the suspension near the wall.

Literature Survey

In this section, the present state of knowledge on the following aspects of CFB technology is presented with specific reference to the experimental observations, modeling approaches, and the assumptions in the development of available models:

- Gas-solid bed structure near the wall
- Particle-convective heat transfer between CFB and a long wall surface
- Radiation heat transfer between CFB and a long wall surface.

Gas-solid bed structure near the wall

The successful operation of a fluidized bed maintaining a densely fluidized state of gas-solid flow with gas velocity higher than the terminal velocity of the mean particle size led to the concept of aggregation of the particles in clusters and strands (Yerushalmi, 1978). In the initial stages of the CFB investigations, the mean bed void fraction was described as a function of the gas velocity and solid rate in the fluidization regime diagram. This mean bed void fraction was obtained by averaging over the entire volume of the CFB riser column, assuming no variation along the bed height. This school of thought considered that the clusters were distributed uniformly over the bed volume.

It later was shown by Li and Kwauk (1980), however, that

the cross-sectional mean void fraction varied along the height. Through further research and extensive experimental investigations, several researchers have agreed on the definition of the CFB operating regime: fast fluidization as "steady cocurrent upflow of a gas-solid mixture with the existence of a relatively denser bed at the lower part coexisting with a dilute suspension at the top end," which was proposed by Takeuchi et al. (1986). This definition has also been recommended by Matsen (1988).

A second school of thought described the solids distribution in the dilute entrained section of the top of the riser as a dilute core surrounded by a denser annular layer of solids, originally proposed by Gagdos and Bierl (1978) based on their own data, as reported by Dry (1987). Other experimental findings of Weinstein et al. (1986), Dry (1987), Bader et al. (1988), Horio et al. (1988) confirm the second school of thought: lean core/dense annulus bed structure for the upper part of the CFB riser.

The bed structure near the wall in the upper part of the laboratory-scale CFB riser was investigated by Bolton and Davidson (1988) and Rhodes et al. (1988). They reported that the layer of particles near the bed wall move downward, and the flow rate of the wall layer increases exponentially with distance from the top of the riser. This suggests that the wall layer grows in its thickness as it moves down. The observed thickness of the wall layer varied from several millimeters to several centimeters. Further, the voidage of this layer was experimentally estimated to be in the range of 0.7–0.8. The fiber optic probe study of the CFB structure by Horio et al. (1988) confirms this, as well as the existence of clusters in the lean core with their size in the range of few millimeters which remained constant throughout the column height. Thus, it is clear that the bed structure adjacent to the wall differs distinctly from that of the lean core. The only direct measurement on a large-scale CFB combustor reported by Schaub et al. (1989) confirms this type of flow structure. It also was observed that the core annulus feature of a CFB might not be related strongly to the bed size (Horio, 1990).

Accordingly, the gas-solid bed structure for a CFB operating in the fast fluidization regime can be redefined as "a denser bottom zone that has an average bed void fraction of about 0.7 and a dilute entrained upper zone that has a lean core with an average void fraction exceeding 0.9 and a denser annulus with an average void fraction in the range of 0.7–0.8." To model the heat transfer process between a CFB and a wall surface, it is very important to model first the wall layer based on its structure and dynamics.

Particle-convective heat transfer between CFB and long wall surface

Glicksman (1988) reviewed the experimental results of CFB heat transfer for both long and short heat transfer probes. Table 1 shows the only available experimental data on heat transfer between a long wall surface and a CFB. Even these laboratory-scale studies are available only for a maximum length of about 1.6 m. The data show a continuous decrease in the value of the local heat transfer coefficient along the distance measured from the top of the heat transfer surface. However, while the Wu et al. data (1987) indicate a linear decrease, the more detailed measurements of Wu et al. (1989) indicate a nonlinear variation with a rapid decrease over the initial portion of the distance that gradually reaches an asymptotic value. It was suggested that the possible reason for this decrease could be the continuous downward movement of the particle layer near the wall. The Wu et al. measurements (1987) made at bed temperatures of 463 K and 513 K can be considered justifiably to be the particle-convective component.

Subbarao and Basu (1986) assumed that the heat transfer in a CFB could be modeled on the lines of the surface renewal theory of a bubbling fluidized bed. They proposed that the bed consists of particle clusters and bubbles that transfer heat by transient conduction to the surface. The particle-convective component h_{pc} was then defined as the weighted average of the cluster contribution h_c and the bubble contribution h_b in the following form:

$$h_{pC} = h_c \delta_c + h_b (1 - \delta_c) \tag{1}$$

where δ_c is the fraction of the surface covered by the clusters. Because of the lack of information on δ_c for the fast fluidized condition of a CFB, they used Matsen correlation (1982) developed for a slugging bed to estimate the value of δ_c. Therefore, they compared the model predictions with Fraley et al.'s low-temperature data (1983) for a 0.95-cm-OD, 15-cm-long heater kept close to the wall of a 7.5-cm-dia. slugging bed and reported satisfactory agreement.

Table 1. Published Experimental Studies on Long Bed Wall Surface Heat Transfer in CFB

Authors	Wu et al. (1987)	Wu et al. (1989)
	CFB Column	
Bed Cross Section (m × m)	0.152 × 152	0.152 × 0.152
Height (m)	7.3	7.3
	Heat Transfer Surface	
Type	Membrane Wall	Membrane Wall
Tube OD (m)	0.0213	0.0213
Tube Length (m)	1.53	1.59
	Particles	
Type	Sand	Sand
Mean Dia. (μm)	188–356	222–299
Density (kg/m^3)	2,637 2,642	3,066
	Operating Conditions	
Pressure (bar)	1	1
Sup. Gas Vel. (m/s)	4–7	6.5–10
Bulk Temp. (K)	423–673	613–1,153

Basu and Nag (1987) improved the Subbarao and Basu model (1986) by incorporating the following changes:

- Contact resistance on the wall due to a gas film of thickness proportional to the particle diameter to effect the particle size of heat transfer
- Replacing the bubble component h_b by the Wen and Miller correlation (1961) for dilute-phase heat transfer
- Correction factor x, which represents the ratio of solid concentration at the wall to the average bed concentration, to take care of the denser annulus, in the calculation of δ_c.

They said that with these changes the model could predict the physical behavior of the heat transfer in fast fluidized beds. They reported that the model predictions agreed satisfactorily with their short (2.5-cm-dia.) heat transfer probe data and those of Fraley et al. (1983). However, this model did not consider the influence of the length of the heat transfer surface. The appropriateness of this cluster and bubble approach of the above two studies is to be examined further, in view of the improved understanding on the gas-solid bed structure near the bed wall from the experimental results available.

Glicksman (1988) proposed that the heat is transferred across a film of particles of constant thickness equal to four particle diameters by unsteady conduction. By considering further a gas layer between the surface and the film, the overall heat transfer coefficient was estimated:

$$h_0 = \left[\frac{1}{h_w} + \frac{1}{h_H}\right]^{-1} \tag{2}$$

where h_w is the heat transfer coefficient for the gas layer and h_H is the heat transfer coefficient for transient conduction to the homogeneous semi-infinite medium. The mean contact time required for the evaluation of h_H was related to the falling film displacement. The solution of the equation, which relates the contact time with the falling film displacement, required the maximum value of the particle velocity. Assuming typical values of 1, 2, and 5 m/s for the maximum particle velocity with a film thickness of 400 μm for a 100-μm particle size, heat transfer coefficients were reported for various values of the vertical distance measured from the top. The heat transfer coefficient continuously decreased along the surface. The results were compared with the experimental data of Wu et al. (1987), which showed large deviations when the length exceeded 40 cm. It is not certain whether transient conduction mechanism can be applied to a long wall with very high contact times and whether constant film thickness assumption is justified in view of the recent experimental evidence of growing wall layer.

Radiation heat transfer betwen CFB and a long wall surface

Grace (1986) recommended the use of Stefan Boltzman equation for the estimation of the radiation component h_r by treating the suspension as a gray body. He also suggested that the suspension emissivity can be approximated as an average between the particle emissivity and a value of unity. He estimated h_r to be 84 W/m^2·K (at the bed temperature of 1,123 K, the surface temperature of 473 K, the surface emissivity of 0.78, and the particle emissivity of 0.52).

Basu and Nag (1987) also used the same approach in their model and approximated the radiation from the entire bed as that from the clusters in contact with the wall. The model overpredicted the high-temperature data by about 25–30% for a short heat transfer surface (10-cm-long) of Kobro and Brerton (1986). The low-heat transfer coefficients observed experimentally were attributed to the effect of a cool wall opposite to the heat transfer probe. Since the heat transfer probe itself was arranged as an annular ring forming the bed wall, this reasoning is not entirely convincing.

Basu and Konuche (1988) considered the suspension emissivity to be a weighted average of the emissivity of the cluster and that of the dispersed phase. They reported fair agreement between the predictions of this model and their own high-temperature data for a short heat transfer probe in a CFB operating at the low suspension density value of about 20 kg/m^3 and the superficial gas velocity of 8–11 m/s. The h_r values varied from 60 to 140 W/m^2·K when the suspension temperature was changed from 923 K to 1,153 K at a constant suspension density of 20 kg/m^3. The h_r value of 84 W/m^2·K obtained by Grace (1986) appears to be quite reasonable under those operating conditions. The h_r value of 140 W/m^2·K given by Basu and Konuche (1988) appears to be quite high. However, this may be attributed to the nature of gas-solid flow under the conditions given. The gas velocity of 8–11 m/s for a particle size of 296 μm will have a saturation-carrying capacity which is higher than the solids circulation flux that actually exists in the bed at this suspension density. It would mean that the bed actually is in a pneumatic transport condition, rather than in a fast fluidization condition. In the pneumatic transport mode, the overall emissivity of the particles could be greater than 0.95 (Glicksman, 1988), and the wall surface is exposed directly to the core without any intervening emulsion layer. This situation might lead to the high radiative heat transfer coefficient values.

All of the above work on h_r have been carried out essentially for a short heat transfer probe. For a long vertical-bed wall surface, appreciable particle cooling can be expected as it flows over the surface with a reduction in h_r values, especially when the nonlinear nature of radiation is considered.

Rationale and Scope of the Present Model

Using the information available from laboratory- and large-scale CFB studies, a realistic heat transfer model should consider the core-annulus type of flow structure, suitably accounting for the layer's growth during its downward movement. The present work considers the core-annulus bed structure to develop a wall layer model, whose results are used as inputs into an available heat transfer model appropriate for the existing conditions.

The Model

Wall emulsion layer

The physical model for the layer is shown in Figure 1. From the earlier observations, it can be conceptualized that an emulsion layer originates at the riser top and grows downward along the wall surface due to the lateral migration of the particles from the core when the solids circulation flux exceeds the saturation-carrying capacity of the gas. The downward flow of the emulsion layer is assumed to be laminar, since the Reyn-

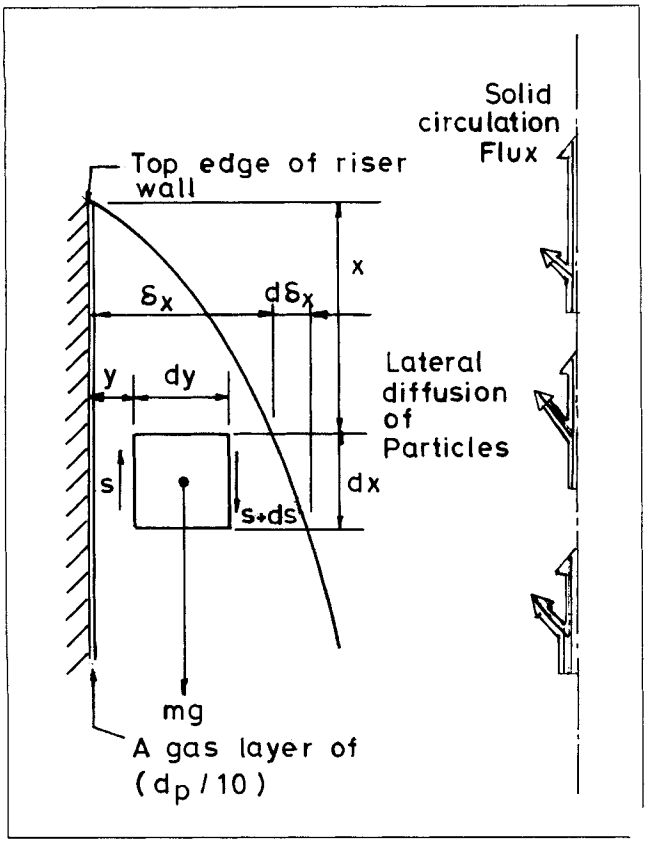

Figure 1. Physical model of the developing emulsion layer.

olds number based on the layer thickness is less than 1,000. This value was used based on the transition criterion of falling liquid films (Bird et al., 1960), due to the lack of better criterion for the present condition.

The operational feedback of CFB combustors (Weimer et al., 1990) reveals that there is very little erosive wear of the major portion of vertical water wall surfaces. This means that either very few particles touch the wall or the particle velocity adjacent to the wall is not very significant.

Consequently, a gas gap of $d_p/10$ between the layer and the surface is assumed, and therefore a no-slip condition for the gas (which is a part of the emulsion) at the wall. The layer properties are determined by the standard method of combining the gas and solid properties in a weighted fashion. The layer voidage is assumed to be 0.7 based on the experimental observations of Bader et al. (1988) and Weinstein et al. (1986). The experimental data reported by Horio et al. (1988) on the layer voidage at various elevations reveal that there is no appreciable variation between the two voidage values at 1.06 m and 1.63 m. It prompts us to assume a constant voidage value. According to the available literature, viscosity of the downward flowing mixture of gas and solids is a "difficult-to-ascertain" parameter, and as a first step, it is taken to be 0.1 Ns/m^2 as suggested by Kunii and Levenspiel (1969) for bubbling fluidized beds.

In the core, there exists a longitudinal decay of entrainment flux above the bed surface. This necessitates the lateral diffusion of particles from the core to the wall resulting in the growth of the layer as it moves down. The change in the thickness of the emulsion layer is related to the difference between the local entrainment flux and the solid circulation flux. As the emulsion layer moves downward from x to $x+dx$, the thickness of the emulsion layer grows from δ_x to $\delta_x + d\delta_x$. A force balance over an elemental volume of $(dx)(dy)$ (1) in the emulsion layer will result in the following governing equation, neglecting the inertia effects:

$$(d^2v_x/dy^2) = -(\rho_e g/\mu_e) \tag{3}$$

where $\rho_e = \rho_p(1-\epsilon)$.
The boundary conditions are:

$$v_x = 0 \quad \text{at} \quad y = 0$$
$$\frac{dv_x}{dy} = 0 \quad \text{at} \quad y = \delta_x \tag{4}$$

Solution of Eq. 3 subject to the boundary conditions (Eq. 4) results in a parabolic velocity profile given by:

$$v_x = \frac{\rho_e g \delta_x}{\mu_e} y - \frac{\rho_e g}{\mu_e} \frac{y^2}{2} \tag{5}$$

The mean flow velocity is obtained by integration of Eq. 5 and upon substitution of limits as:

$$\bar{v}_x = \frac{\rho_e g \delta_x^2}{3\mu_e} \tag{6}$$

The mass of emulsion flowing per unit time per unit width through the cross section at x is determined as:

$$G_x = \frac{\rho_e^2 g \delta_x^3}{3\mu_e} \tag{7}$$

This mass flow rate of emulsion is equal to that arising due to the lateral migration of particles from the core, in the region of the riser wall section between the top edge and the local station at x. Expressing this mass flow rate in terms of entrainment at the section x, E_x, and the entrainment at the riser exit that is the solid circulation flux, G_s, we have the following equation:

$$G_x = \frac{(E_x - G_x)A}{f \cdot P} \tag{8}$$

where f is the fraction of the wall surface covered by the wall layer that depends on the superficial gas velocity, particle size, solid circulation flux, the bed size, and the wall geometry. As the prediction of this 'f' value is not possible with the present state of knowledge of the bed dynamics, in the present work it is taken as 1, which means that the entire heat transfer surface is uniformly covered by a continuous emulsion layer.

Comparison of Eqs. 7 and 8 yields an expression for the local thickness of the emulsion layer as:

$$\delta_x = \left[\frac{3\mu_e(E_x - G_s)A}{gP\rho_e^2 f}\right]^{1/3} \tag{9}$$

The value of E_x is obtained by following the Wen and Chen correlation (1982) developed for a bubbling fluidized bed with a value of $a=0.5$, as suggested by Rhodes and Geldart (1987) for application to CFB in the following form:

$$E_x = E_\infty + [E_0 - E_\infty]\exp(-a(\ell - x)) \tag{10}$$

The value of ℓ can be obtained by substituting the solid circulation flux G_s for E_x and zero for x, given the values of E_o, E_∞ and "a".

Particle-convective component (h_{pc})

Yoshida et al. (1969) proposed a mechanism of heat transfer between bubbling fluidized beds and long wall surfaces by considering that a thin layer of emulsion contacted the surface during a time 't' after which a fresh layer replaced the previous one. When the contact time is very short, heat transfer occurs by unsteady conduction from the emulsion layer to the surface; and for very long contact times, heat transfer occurs by steady-state conduction. In the case of intermediate contact times, both the mechanisms come into play. In the present model, the wall layer between the top edge and the local station at x is considered analogous to the emulsion layer of Yoshida et al. (1969), and the contact time is taken to be its travel time along the surface. Considering further the heat transfer mechanism to be the same as given by them for intermediate contact times, the following solution for the instantaneous local heat transfer coefficient is adopted for the present model:

$$h_x = \frac{k_e}{\delta_x} + 2\frac{k_e}{\delta_x}\sum_{i=1}^{\infty}\exp\left\{\frac{-i^2\pi^2\alpha_e t}{\delta_x^2}\right\} \tag{11}$$

where $\alpha_e = k_e/\rho_e C_{pe}$, and k_e is calculated using the expression recommended by Gelperin and Einstein (1971). The emulsion layer contact time is estimated from the following relation:

$$t = \frac{x}{v_x} \tag{12}$$

In case the heat transfer surface does not originate at the top edge of the riser wall, x is to be replaced by $(x - x_0)$ in Eq. 12 where x_0 is the uncooled height preceding the heat transfer surface. The heat transfer coefficient at a given location is calculated by assuming an emulsion layer of length x starting from the riser top using appropriate values of t from Eq. 12 and δ_x from Eq. 9. This procedure of calculating the local values in a progressive fashion, which starts from the top edge of the riser, indirectly accounts for the change in the internal energy across the emulsion layer in the vertical direction. It is assumed that the thermal depth and the physical depth are equal for the emulsion layer all along the heat transfer surface as the Prandtl number of the emulsion layer is of the same order as that of air. The local particle-convective component h_{pc} is written finally as the sum of the gas layer resistance at the wall and that of the moving emulsion layer in the form:

$$h_{pc} = \frac{1}{\left[\frac{d_p}{10k_g}\right] + \left[\frac{1}{h_x}\right]} \tag{13}$$

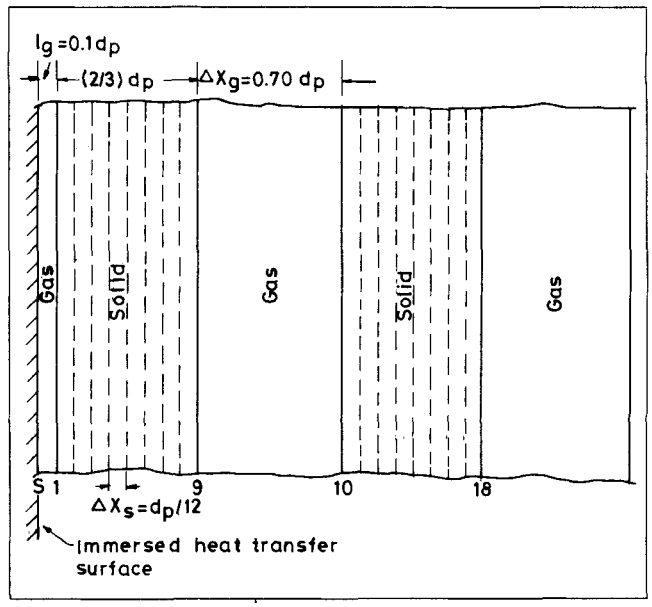

Figure 2. Physical model for radiation.

Radiation component (h_r)

The physical model for the radiation is shown in Figure 2, which is an adoption of the Kolar et al. model (1979) for the CFB wall heat transfer. In the present work, the gas slab thickness between two successive solid slabs is taken as a fitting parameter, and a best fit value of 0.7 d_p is obtained from the high-temperature experimental data of Wu et al. (1989). The emissivity of the particle is taken as 0.7 from Basu and Konuche (1988). The calculation procedure is the same as that of Kolar et al. (1979). The above procedure yields the length-averaged value for the radiation component from which the local value of h_r is deduced.

Results and Discussion

In the CFB heat transfer literature, most of the heat transfer data are reported using the bed suspension density as the main variable. While the suspension density varies very little axially in the entrained zone, there is a very substantial density change in the radial direction. The density remains essentially constant (equivalent to a voidage greater than 0.9) in the core and drastically increases to a higher value (equivalent to a voidage of about 0.7) in a few-centimeters thick zone adjacent to the wall. Thus, the density used in the literature is a cross-sectional-area-averaged value. The suspension density is not an independently controlled variable, which depends on the solid circulation flux, the particle diameter, and the superficial gas velocity. Therefore, for a meaningful comparison of models and various data, solid circulation flux and the superficial gas velocity must be the same for a given particle diameter. In addition, the knowledge of suspension density alone cannot indicate whether the CFB is in the fast fluidization regime, whereas a combination of G_s and U indicates the existence (or nonexistence) of the fast fluidization regime. In the reported literature, these independent variables are not often available. For these reasons, comparisons are here made between the present model predictions and the available data wherever possible extracting required information from graphs.

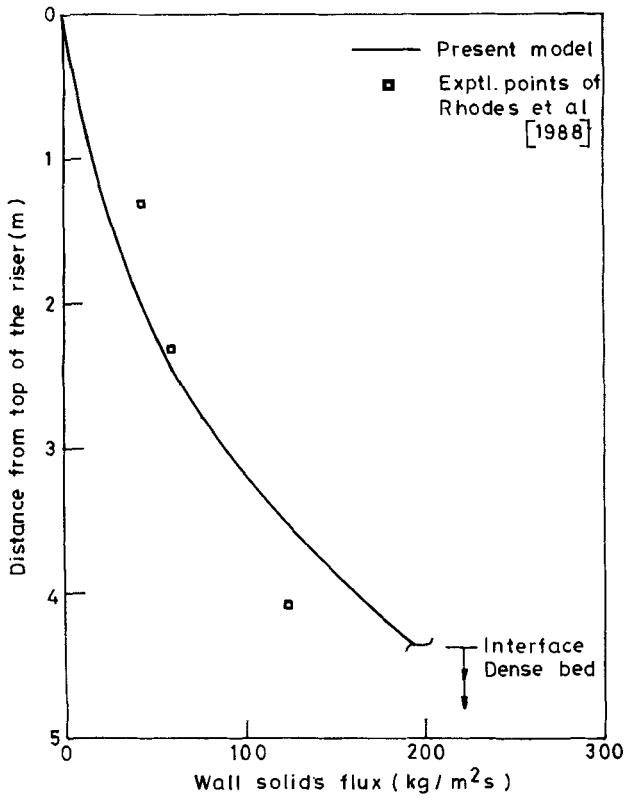

Figure 3. Wall solids flow rate as a function of downward distance from riser top.

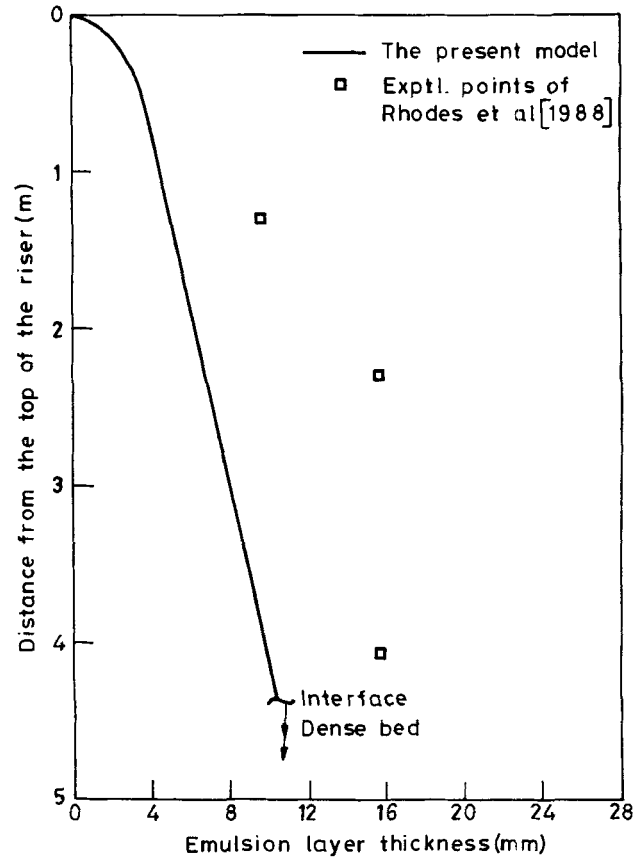

Figure 4. Thickness of the wall layer as a function of downward distance from riser top

To investigate the applicability of the present model, its predictions are compared with the relevant experimental data of Rhodes et al. (1988), Wu et al. (1987, 1989), Kobro and Brerton (1986), Basu and Nag (1987), and Basu and Konuche (1988). The influence of G_s, T_{sus}, L, U and d_P on emulsion layer characteristics and heat transfer are presented here, and the present model predictions are compared with other model predictions.

Wall emulsion layer model predictions

The wall emulsion layer model presented here gives an expression for the wall layer thickness. The wall layer solids flow rate is required to estimate the layer thickness and the difference between the local entrainment flux and the solid circulation flux. Figure 3 presents the model predictions of the downward solids flow rate along the wall in the entrained zone for the experimental conditions of Rhodes et al. (1988). The experimental points deduced from the graph presented in Rhodes et al. (1988) are also shown in the figure. The flow rate decreases with increase in the distance from the distributor plate. Considering the assumptions in the model and the uncertainties involved in the extraction of experimental data, the model predictions show a reasonably good agreement with the data both qualitatively and quantitatively. A more thorough comparison will be possible when more relevant data are available.

Figure 4 presents the thickness of the wall layer as predicted by this model corresponding to the experimental conditions of Rhodes et al. (1988). It can be seen that the layer originates at the riser top which is 4.37 m from the interface, attains a thickness of about 3 mm (47 d_p) within a distance of 37 cm, and then gradually increases to about 1 cm (156 d_p) at the interface. The model underpredicts the layer thickness by about 40–60%. It is interesting to note that the experiments offer an almost constant thickness for the layer in the bottom half of the dilute-entrained zone even though the solids flux has changed substantially as seen from Figure 3.

Emulsion layer profiles as predicted by this model for typical laboratory experimental conditions (200-μm-dia. sand particles, fluidizing air at 373 K, a bed size of 15.2 cm × 15.2 cm, and a superficial gas velocity of 5.5 m/s) are shown in Figure 5. The solid circulation flux is varied in the realistic range of 20–70 kg/m^2·s. The wall layer thickness increases along the surface for a given value of G_s, the thickness being greater for larger G_s values. However, the maximum thickness, which occurs at the interface, shows very little variation and needs experimental corroboration. The layer profiles in the figure also show that the interface moves up higher in the bed with increased G_s values. It is also observed as expected that the rate of increase in the layer thickness and the interface height reduces with the increase in G_s value.

Figure 6 presents the emulsion layer profiles as predicted by this model corresponding to the experimental conditions (463 K, $G_s = 28$ kg/m^2·s) of Wu et al. (1987). The superficial gas velocity is varied in the realistic range of 4–8 m/s. It is seen that the layer thickness increases along the surface for a given value of U. The thickness, however, decreases at a given lo-

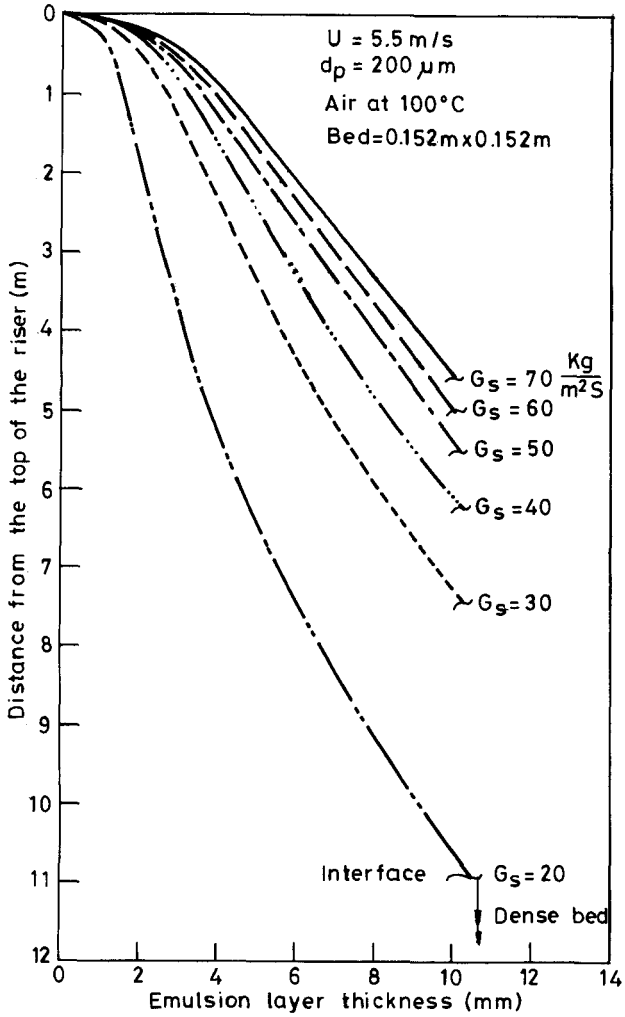

Figure 5. Emulsion layer profiles as a function of distance from riser top and solid circulation flux.

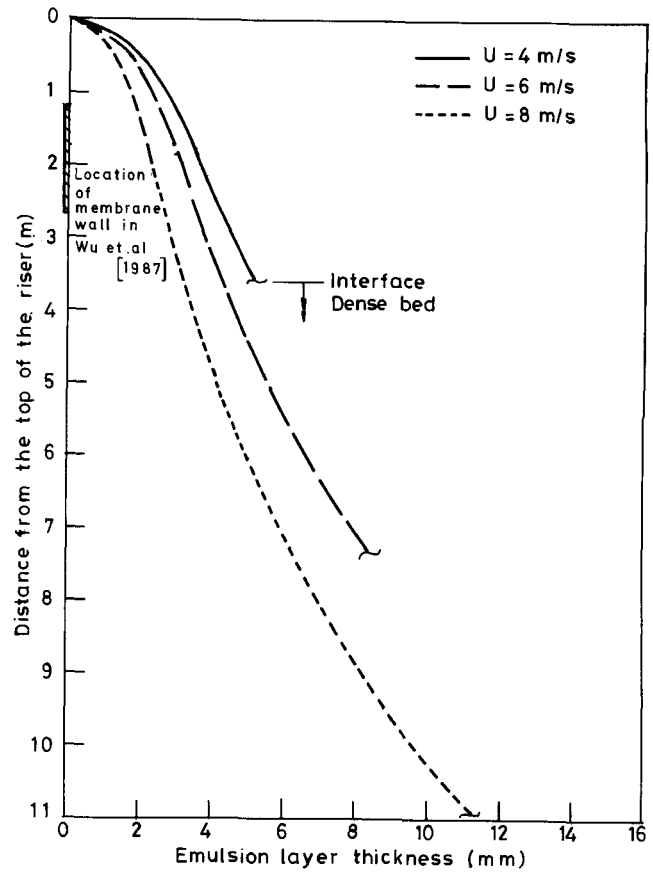

Figure 6. Emulsion layer profiles as a function of the distance from riser top and superficial velocity (G_s = 28 kg/m²·s).

cation for increasing U values. This is physically convincing, since, as U increases, the saturation-carrying capacity of the gas increases, thus reducing the mass flow rate of solids toward the wall resulting in a decrease in the wall layer thickness.

The mean solids velocity obtained from Eq. 6 based on the emulsion layer thickness is in the range of 0.1 to 2.0 m/s for the normal operating conditions.

The effect of a change in the layer voidage on the layer thickness is also investigated, and the calculations show that by increasing the voidage from 0.7 to 0.8, the emulsion layer thickness at a distance of about 1.58 m from the heater top increases from 3.8 mm to 5 mm.

The present wall layer model can bring out the scaling effect through Eq. 9, which predicts that the thickness of the emulsion layer increases according to the cube root of the column diameter. It is appropriate to mention here that the present model predicts changing dimensionless core diameter, while Horio's and Glicksman's scaling laws maintain a constant dimensionless core diameter when the bed size is scaled up.

Heat transfer

The wall emulsion layer model developed will be used now to predict the heat transfer coefficient component h_{pc}, along with the alternate slab model to predict h_r, as functions of the important operating variables. Comparisons will be made with the other available model predictions and experimental data.

Effect of Solid Circulation Flux. For a comparison of the heat transfer model predictions for a long vertical wall surface, the data of Wu et al. (1987, 1989) are the only available one in the literature. The emulsion layer thickness required for the model for the operating conditions of Wu et al. (1987) is shown in Figure 7, as well as the actual location of the surface in the experiments relative to the emulsion layer. For these conditions, the emulsion layer thickness has a maximum value of about 7.7 mm at the interface for G_s = 28 kg/m²·s, and for G_s = 69 kg/m²·s it has 7.3 mm. The heat transfer surface for the latter case is just above the interface with a very large layer thickness, whereas for the lower G_s value, the heat transfer surface is well above the interface and the layer thickness is relatively smaller.

The effect of the change in layer thickness on heat transfer is shown in Figure 8, which shows the variation of the local total heat transfer coefficient along the surface. Higher G_s condition results in a higher heat transfer coefficient because of the heat input brought about by the lateral diffusion of particles from the core, at which a higher suspension density condition exists. This fact is in accordance with the previously reported findings of Grace (1986). The model predictions agree very well with the experimental data both qualitatively and

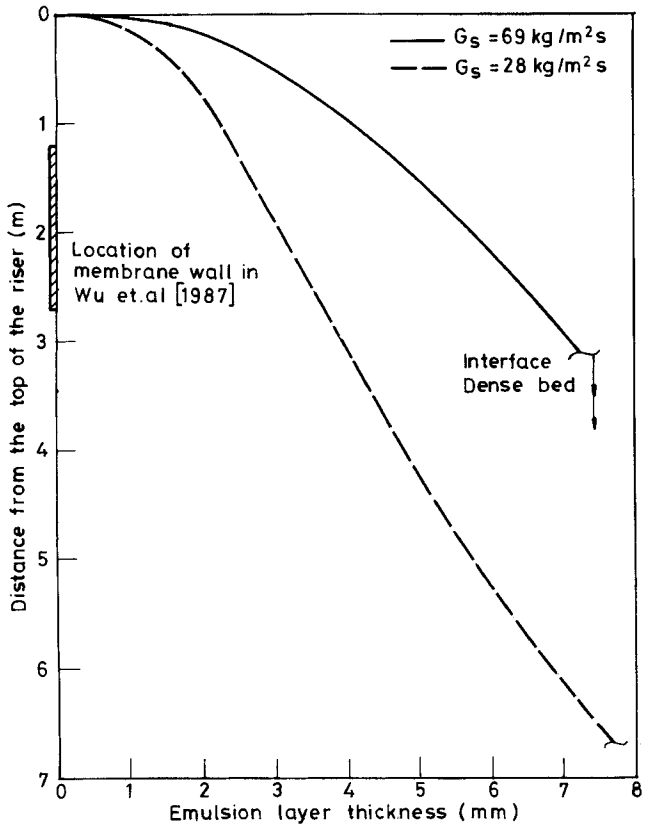

Figure 7. Emulsion layer thickness as a function of distance from riser top and solid circulation flux.

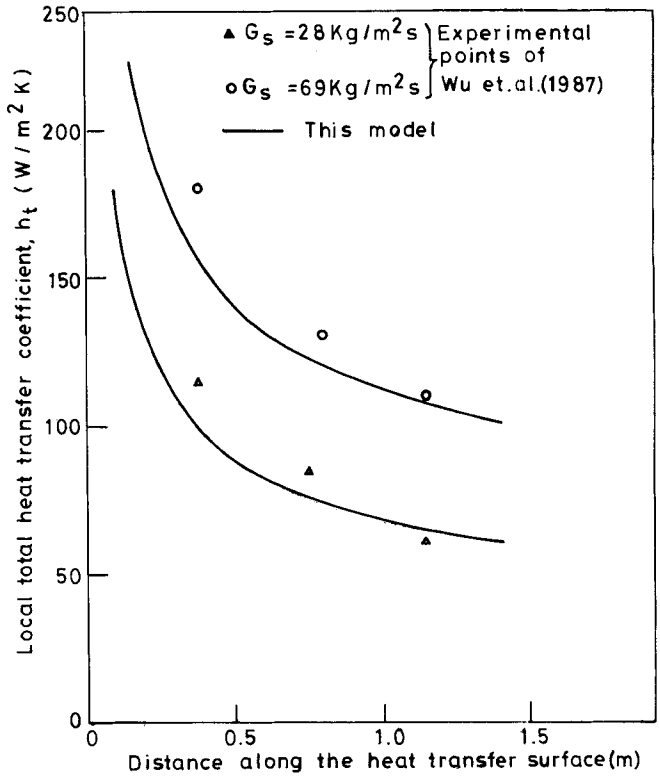

Figure 8. Effect of solid circulation flux on local heat transfer coefficient along heat transfer surface.

quantitatively. The experimental points suggest a nearly linear variation of the local heat transfer coefficient with the distance, while the model predicts an initial rapid decrease gradually reaching an asymptotic value. The root mean square deviation of the experimental data points from the model predictions is of the order of 10%.

Wu et al. (1989) reported more extensive data for local heat transfer coefficient variation on a 1.59-m-long bed wall surface for a suspension temperature of 680 K as shown in Figure 9. The experimental data show a nonlinear decrease in the heat transfer coefficient as opposed to the nearly linear characteristic shown in Figure 8. As can be seen, the model predicts the data both qualitatively and quantitatively with very little deviation.

The Glicksman model incorporates the influence of the surface length on the heat transfer coefficient, and hence it should give variation in the heat transfer coefficient. It has not been possible to calculate the heat transfer coefficient for the Wu et al. experimental condition (1987) from this model, since it requires more details of the model than given by Glicksman in 1988. Although the Basu and Nag model (1987) does not consider the influence of the surface length, their model prediction is shown in the figure. Clearly, this model underpredicts the experimental values at short distances.

Effect of Suspension Temperature. Figure 9 presents the variation of the local total heat transfer coefficient along the surface for two different suspension temperatures: 680 K and 1,133 K. The h_t value is calculated as two components: the first one h_{pc} and the second, h_r, both of which are explained in the previous sections. The agreement between the model predictions and the experimental data, both at lower and higher temperatures, is very good. As stated earlier, it is noted that the h_t values at 1,133 K contain a radiation component h_r calculated by the alternate slab model, whose variation is also shown in the figure.

An interesting fact is the gradual decrease of h_r along the heat transfer surface, which agrees with the observations of Glicksman (1988). This is due to the first layer of particles adjacent to the wall getting cooled as it moves down. It is interesting to note the extent of particle cooling during its downward movement, which is the same for the present alternate slab model predictions in Figure 10. This clearly explains why radiation has very little effect when the surface length increases. The h_r values are quite low over the major portion of the surface even at very high suspension temperatures, while they could be of the order of 50–70 W/m²·K for very small heat transfer probes when the suspension density is 54 kg/m³. Note that the high-temperature data of Basu and Konuchue (1988) are for very low suspension densities in the range of 20 to 30 kg/m³ and in which reported h_r values are in the range of 60–140 W/m²·K.

Wu et al. (1989) reported that the difference between heat transfer coefficient values at 680 K and 1,133 K represents the contribution of the radiation in the range of 30–40% of h_t. However, the increase in the heat transfer coefficient obtained for the higher operating temperature is contributed to: (1) the increase in the particle-convective component due to a higher thermal conductivity of the gas and (2) the radiation. To separate the radiation contribution it is necessary to quantify the increase in the particle convective component.

Figure 11 shows the emulsion layer model predictions of the

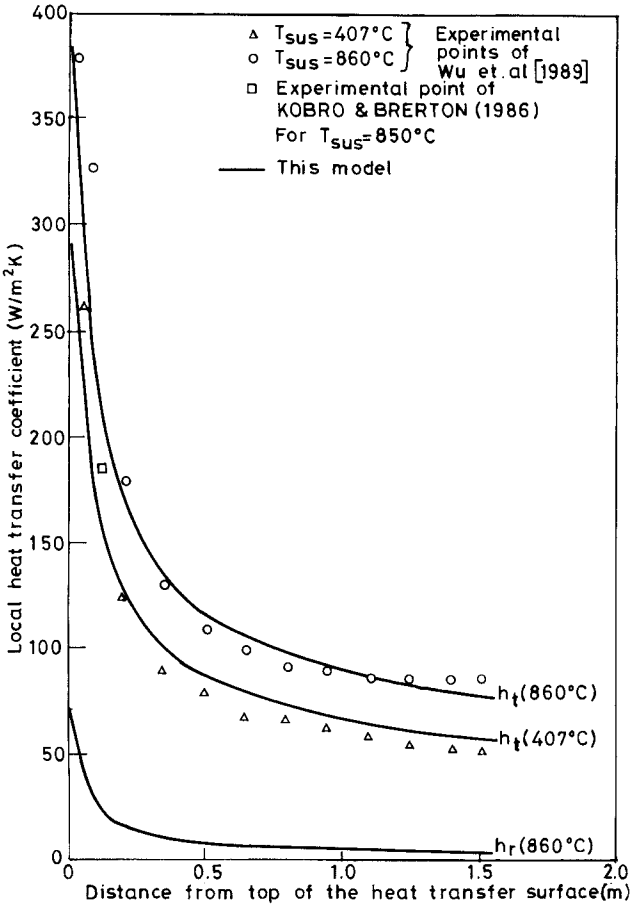

Figure 9. Effect of suspension temperature on local total heat transfer coefficient along heat transfer surface

Suspension density = 54 kg/m^3

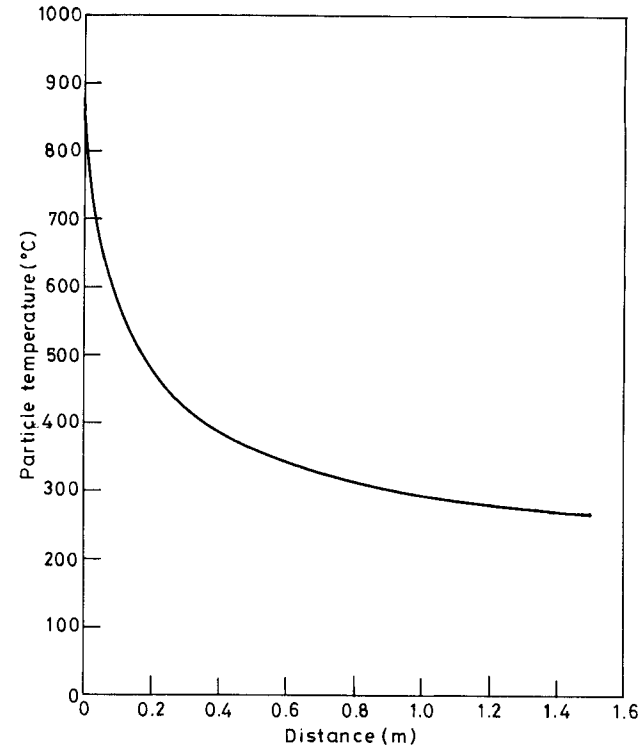

Figure 10. Variation of first-layer particle temperature as it moves down

T_{sus} = 1,173 K

particle-convective component for a temperature range of 473 and 1,133 K for the experimental conditions of Wu et al. (1989). It is shown that there is a definite increase in the h_{pc} value with the increased gas thermal conductivity at higher temperatures. A break-up of the h_{pc} and h_r contributions for Wu et al. (1989) operating conditions are presented in Table 2, which shows that a major share of the increase is due to the increase in h_{pc}; for example, at $x = 0.065$ m the radiation contribution is only 51 W/m^2·K, instead of 117 W/m^2·K as proposed by Wu et al. (1989). This implies that the radiative contribution is of the order of 13.5%, not 31%. Under these conditions, the h_r share is about 5 to 13.5% over the length of the surface. The comparison between the radiation component predicted by the alternate slab model and the experimental h_r values shows a reasonably good agreement, both qualitatively and quantitatively.

Compared also are the h_t values of 185 W/m^2·K for a 10-cm-long surface at 1,123 K interpolated from Kobro and Brerton's graph (1986) (which presents the h_t variation with suspension density). Since the exact location of the heat transfer surface in the experiments of Kobro and Brerton (1986) is not known, it is assumed to be similar to that of Wu et al. (1989). For this condition, a h_t value of 228.8 W/m^2·K can be read off from the curve for 1,133 K in the figure which is an overprediction by about 24%. It is interesting to note here that the model of Basu and Nag (1987) overpredicts the same data point by about 30%.

Figure 12 shows the variation of the distance-averaged total heat transfer coefficient along the surface for the suspension temperatures of 680 K and 1,133 K. The present model predictions follow the trend of the experimental data very well.

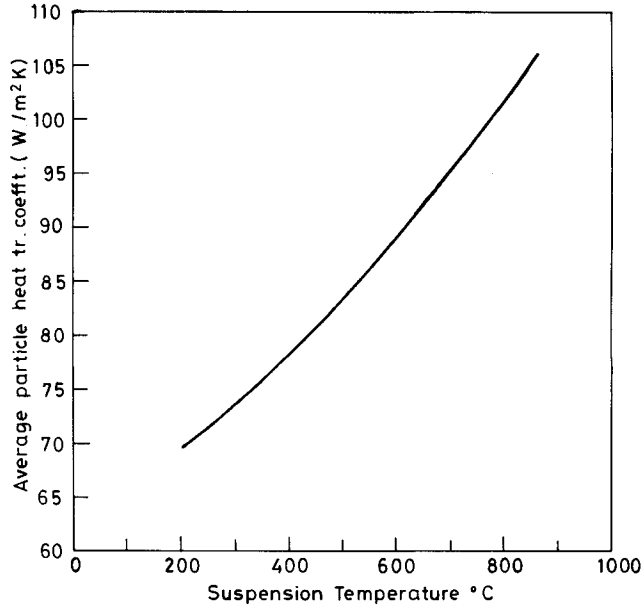

Figure 11. Effect of suspension temperature on average particle-convective heat transfer coefficient.

Table 2. Relative Contribution of Radiative and Particle-Convective Components

Distance (m)	Wu et al. 1989 Exp. Data h_t (W/m²·K) 860°C	407°C	Δh_t	Present Model h_{pc} (W/m²·K) 860°C	407°C	Δh_{pc}	h_t, exp. $\Delta h_t - \Delta h_{pc}$ W/m²·K	h_r Alt. Slab Model W/m²·K
0.065	380	263	117	301	235	66	51	46
0.205	180	125	55	162	125	37	18	16
0.355	132	90	42	133	98	35	7	13
0.505	108	75	33	112	85	27	6	9.9
0.6525	100	67	33	104	77	27	6	9.5
0.7975	94	64	30	95	71	24	6	8.1
0.945	90	60	30	90	67	23	7	6.9
1.095	88	60	28	86	63	23	5	6.1
1.245	87	55	32	83	60	23	9	4.9
1.3925	87	54	33	80	58	22	11	4.7
1.5275	86	58	28	77	58	19	9	4.2

The agreement between the predictions and the data is generally satisfactory, and it improves longer wall surfaces.

Following the explanations given earlier, it is calculated that the radiation contribution in the distance-averaged total heat transfer coefficient is in the range of 8 to 13% for the operating conditions of Wu et al. (1989).

Effect of Heat Transfer Surface Length. The influence of the heat transfer surface length, L, on the average value of h_{pc} as predicted by the present model is shown in Figure 13 with d_p as a parameter. The solid circulation flux values taken in the calculations are different for various particle sizes to get the required height in the dilute-entrained zone. As can be seen, the $\bar{h}_{pc}$ decreases with increasing length of the heat transfer surface. As an example, for a particle size of 200 μm, $G_s = 20$ kg/m²·s and $U = 5.5$ m/s, the $\bar{h}_{pc}$ values are 378 W/m²·K, 168 W/m²·K, 70 W/m²·K and 63 W/m²·K for 1-, 10-, 100- and 1,000-cm-long heat transfer surfaces, respectively.

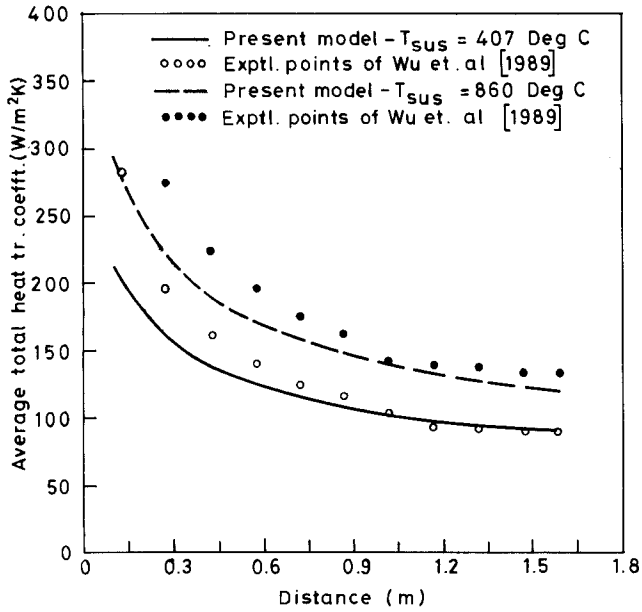

Figure 12. Total heat transfer coefficient averaged up to the distance vs. distance.

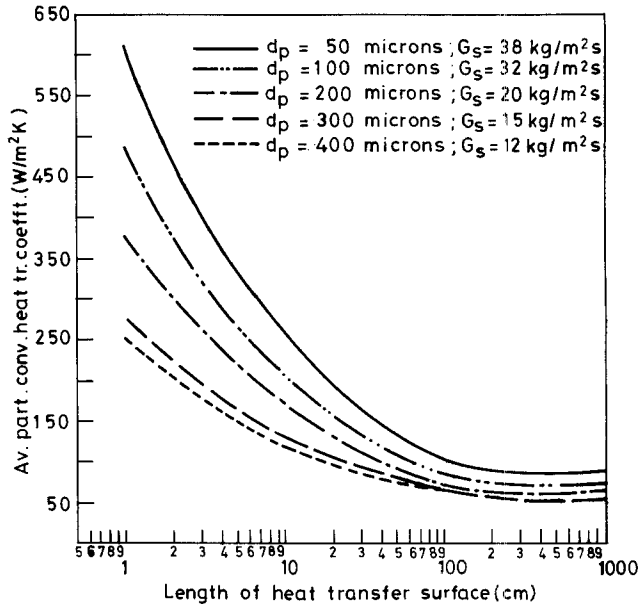

Figure 13. Average particle-convective heat transfer coefficient vs. length of heat transfer surface for various particle diameters.

The $\bar{h}_{pc}$ values decrease very rapidly in the length range of 1-100 cm and show a small variation in the length range of 100-1,000 cm. The effect of particle size is appreciable in the range of 1-100 cm where a large change in the $\bar{h}_{pc}$ occurs. The particle-size effect diminishes when the length increases. It may be noted that the present model predictions closely follow the trend given by Wu et al. (1989) based on the experimental data of several research workers. As observed by Wu et al (1989), the influence of the particle size diminishes with longer surfaces as the contact times on the surface are much higher than the thermal time constants for the entire range of particle sizes considered, 50 μm to 400 μm, whereas the same does not hold good for very short lengths.

Effect of Superficial Gas Velocity. The influence of superficial gas velocity on the h_{pc} value averaged over the 1.53-m-long surface as predicted by the present model is shown in Figure 14 with G_s as a parameter. It is seen that the average h_{pc} decreases by about 30% for $G_s = 28$ kg/m²·s, 15% for $G_s = 35$ kg/m²·s, and 10% for $G_s = 50$ kg/m²·s when the superficial gas velocity is changed from 4 m/s to 8 m/s. This reduction is attributed to the fact that when G_s is held constant, the layer thickness is reduced when the velocity is increased as already shown in Figure 6. For further confirmation of the effect of velocity, the experimental data of Wu et al. (1987) is shown for a constant suspension density value of about 58 kg/m³. The decrease in heat transfer coefficient is about 20%. It implies that the particle-convective component plays a more dominant role than the gas-convective component. This may be attributed to the fact that most of the upward gas flow goes through the core (Bader et al., 1988), and hence any contribution to heat transfer due to gas flow is minimal at the wall surface. This observation supports the assumption made in the development of the present model that the gas-convective component is negligible compared to the particle convective component.

Effect of Particle size. Figure 15 shows the effect of d_p

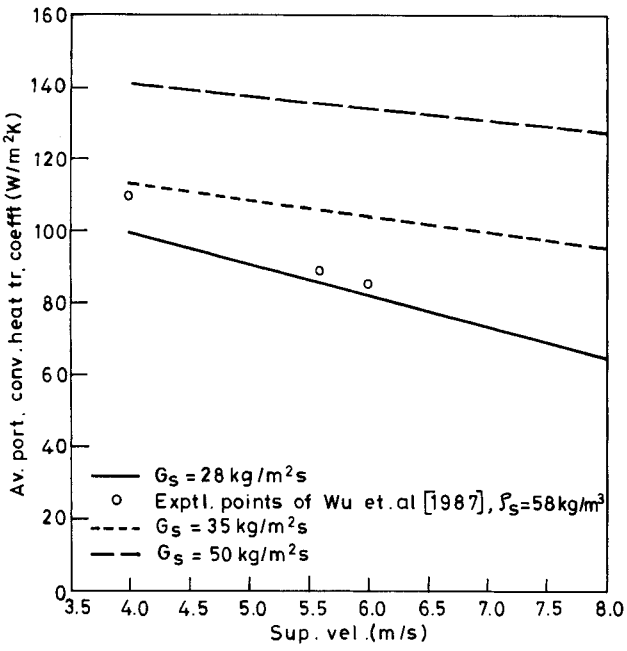

Figure 14. Effect of superficial gas velocity on average particle-convective heat transfer coefficient.

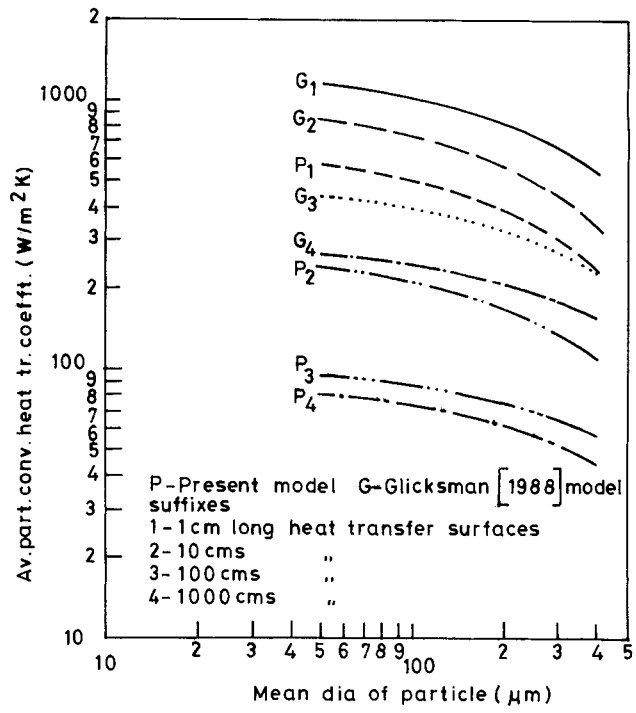

Figure 15. Effect of particle size on the average particle-convective heat transfer coefficient.

variation on the $\bar{h}_{pc}$ with L as a parameter. The $\bar{h}_{pc}$ value decreases when the particle size increases for a given length of the surface. As an example for the 100-cm-long surface, $\bar{h}_{pc}$ values are 103 W/m^2·K, 84 W/m^2·K, 70 W/m^2·K, 64 W/m^2·K, and 63 W/m^2·K for particle sizes of 50 μm, 100 μm, 200 μm, 300 μm, and 400 μm, respectively. The particle size effect is reduced when the heat transfer surface is very long, in the range of 1,000 cm. It agrees with the observations of Glicksman (1988). Also shown in the figure are the predictions of Glicksman (1988) that is an order of magnitude higher than the present model predictions.

Conclusions

- A wall emulsion layer model that predicts the thickness of the downward moving particles along the wall of a CFB has been derived with recent experimental evidence as the basis. The emulsion layer characteristics predicted by the model represent the physics of the CFB dynamics realistically.
- The predictions of a particle-convective heat transfer model, which incorporates both steady-state conduction across the layer and unsteady-state conduction from the layer based on the emulsion layer model, agree very well with the available low-temperature experimental data for vertical wall surface length of about 1.6 m.
- An alternate slab model has been proposed to predict the radiative component for a high-temperature CFB. The overall heat transfer model predictions agree with available high-temperature experimental data, and the overall increase in the heat transfer coefficient at high temperatures is to a large extent due to the increase in the particle-convective component because of the increased thermal conductivity of the gas. Further, the radiation contribution over a 1.6-m-long wall surface is of the order of 8–13% for a CFB operating at about 860°C.
- Based on the present model predictions, the following conclusions could be drawn:

1. The heat transfer coefficient varies directly with solid circulation flux.
2. The decrease in the heat transfer coefficient along the surface is substantial, implying that the surface length is an important parameter.
3. The influence of superficial gas velocity on the particle-convective component is small, especially at higher solid-circulation flux conditions.
4. The particle convective heat transfer increases with decreasing particle size; changing the particle size from 50 μm to 400 μm decreases the $\bar{h}_{pc}$ by about 20–60% for surface lengths ranging from 1 cm to 100 cm and by 15–45% for surface lengths in the range of 100 to 1,000 cm.

Notation

A = cross-sectional area of the riser, m^2
a = constant in Eq. 8
C_p = specific heat, kJ·kg^{-1}·K^{-1}
d_p = mean diameter of particle, m
E = entrainment flux, kg·m^{-2}·s^{-1}
G_s = solid circulation flux, kg·m^{-2}·s^{-1}
G_x = local mass flux per unit width, kg·m^{-1}·s^{-1}
g = acceleration due to gravity, m·s^{-2}
h_{pc} = local particle convective heat transfer coefficient, W·m^{-2}·K^{-1}
$\bar{h}_{pc}$ = average particle-convective heat transfer coefficient, W·m^{-2}·K^{-1}
h_r = local radiative heat transfer coefficient, W·m^{-2}·K^{-1}
h_t = local total heat transfer coefficient, W·m^{-2}·K^{-1}
k = thermal conductivity, W·m^{-1}·K^{-1}
L = length of heat transfer surface, m
ℓ = distance of the interface from riser exit, m
P = perimeter of riser column, m
T_{sus} = temperature of the bed suspension, K
T_w = heat transfer surface temperature, K
t = emulsion layer contact time, s
U = superficial gas velocity, m·s^{-1}

$\bar{v}_x$ = mean velocity of the emulsion at x, $m \cdot s^{-1}$
x = distance measured from the top along the wall, m
x_0 = uncooled distance, m
y = distance measured normal to the wall, m

Greek letters

α = thermal diffusivity
δ_c = fraction of the surface covered by clusters in Eq. 1
δ_x = emulsion layer thickness
ρ = density
μ = absolute viscosity

Subscripts

e = emulsion
g = gas
o = bed surface
p = particle
pc = particle convection
r = radiation
s = solids
t = total
x = local (station of interest)

Literature Cited

Bader, R., J. Findlay, and T. M. Knowlton, "Gas/Solids Flow Patterns in a 30.5-cm-Dia. Circulating Fluidized Bed," *Circulating Fluidized Bed Technology: II*, P. Basu and J. F. Large, eds., p. 123, Pergamon Press, Canada (1988).

Basu, P., and P. K. Nag, "An Investigation into Heat Transfer in Circulating Fluidized Beds," *Int. J. Heat Mass Transfer*, **30**, 2399 (1987).

Basu, P., and F. Konuche, "Radiative Heat Transfer from a Fast Fluidized Bed," *Circulating Fluidized Bed Technology: II*, P. Basu and J. F. Large, eds., p. 245, Pergamon Press, Canada (1988).

Bird, R. B., W. E. Stewart, and E. N. Lightfoot, *Transport Phenomena*, p. 41, Wiley, New York (1960).

Bolton, L. W., and J. F. Davidson, "Recirculation of Particles in Fast Fluidized Risers," *ibid.*, p. 139 (1960).

Dry, R. J., "Radial Particle Size Segregation in a Fast Fluidized Bed," *Powder Technol.*, **52**, 7 (1987).

Fraley, L., Y. Y. Lin, K. H. Hsiao, and A. Solbakken, "Heat Transfer Coefficient in Circulating Bed Reactor," ASME Paper 83-HT-92, Seattle (1983).

Gabor, J. D., "Wall to Bed Heat Transfer in Fluidized and Packed Beds," *Chem. Eng. Symp. Ser.*, **66**, 76 (1970).

Gagdos, L. J., and T. W. Bierl, "Studies in Support of Recirculating Bed Reactors for the Processing of Coal," DOE Contract No. Ex-C-76.01.2449, Report by Carnegie Mellon University, Pittsburgh (Sept., 1978).

Gelperin, N. I., and V. G. Einstein, "Heat Transfer in Fluidized Beds," *Fluidization*, J. F. Davidson and D. Harrison, eds., p. 487, Academic Press, New York (1971).

Glicksman, L. R., "Circulating Fluidized Bed Heat Transfer," *Circulating Fluidized Bed Technology: II*, P. Basu and J. F. Large, eds., p. 13, Pergamon Press, Canada (1988).

Grace, J. R., "Heat Transfer in Circulating Fluidized Beds," *Circulating Fluidized Bed Technology: I*, P. Basu, ed., p. 63, Pergamon Press, Canada (1986).

Horio, M., "Hydrodynamics of Circulating Fluidization: Present Status and Research Needs," Plenary Lecture Preprint, Int. Conf. on CFB, Nagoya, India (1990).

Horio, M., K. Morishita, O. Tachibana, and N. Murata, "Solid Distribution and Movement in Circulating Fluidized Beds," *Circulating Fluidized Bed Technology: II*, P. Basu and J. F. Large, eds., p. 147, Pergamon Press, Canada (1988).

Kobro, H., and C. Brereton, "Control and Fuel Flexibility of Circulating Fluidized Bed," *Circulating Fluidized Bed Technology: I*, P. Basu, eds., p. 263, Pergamon Press, Canada (1986).

Kolar, A. K., N. S. Grewal, and S. C. Saxena, "Investigation of Radiative Contribution in a High Temperature Fluidized Bed Using the Alternate Slab Model," *Int. J. Heat Mass Transfer*, **22**, 1695 (1979).

Kunii, D., and J. M. Smith, "Heat Transfer Characteristics of Porous Rocks," *AIChE J.*, **6**, 71 (1960).

Kunii, D., and O. Levenspiel, *Fluidization Engineering*, Wiley, p. 96 (1969).

Li, Y., and M. Kwauk, "The Dynamics of Fast Fluidization," Int. Fluidization Conf., Henniker, NH (Aug. 3–8, 1980).

Matsen, J. M., "Mechanisms of Choking and Entrainment," *Powder Technol.*, **32**, 21 (1982).

Matsen, J. M., "The Rise and Fall of Recurrent Particles: Hydrodynamics of Circulation," *Circulating Fluidized Bed Technology: II*, P. Basu and J. F. Large, eds., p. 3, Pergamon Press, Canada (1988).

Rhodes, M. J., and D. Geldart, "A Model for the Circulating Fluidized Bed," *Powder Technol.*, **53**, 155 (1987).

Rhodes, M. J., P. Luussman, F. Villain, and D. Geldart, "Measurement of Radial and Axial Solids Flux Variations in the Riser of a Circulating Fluidized Bed," *Circulating Fluidized Bed Technology: II*, P. Basu and J. F. Large, eds., p. 155, Pergamon Press, Canada (1988).

Schaub, G., et al., *Proc. of Int. Conf. on FBC*, p. 685 (1989).

Subbarao, D., and P. Basu, "A Model for Beat Transfer in Circulating Fluidized Beds," *Int. J. Heat Mass Transfer*, **29**, 487 (1986).

Subbarao, D., and P. Basu, "Heat Transfer in Circulating Fluidized Beds," *Circulating Fluidized Bed Technology: I*, P. Basu, ed., p. 281 (1986).

Takeuchi, H., T. Hirama, T. Chiba, J. Biswas, and L. S. Leung, "A Quantitative Definition and Flow Regime Diagram for Fast Fluidization," *Powder Technol.*, **47**, 195 (1986).

Weimer, R. F., A. D. Bixler, R. D. Pettit, and S. I. Wang, "Operation of a 49-MW Circulating Fluidized Bed Combustor," *Int. Conf. on CFB*, preprint p. 1-9-1, Nagoya, Japan (1990).

Weinstein, H., M. Shao, and M. Schnitzlein, "Radial Variation in Solid Density in High-Velocity Fluidization," *Circulating Fluidized Bed Technology: I*, P. Basu, ed., p. 201, Pergamon Press, Canada (1986).

Wen, C. Y., and E. N. Miller, "Heat Transfer in Solids–Gas Transport Lines," *I.E.C.*, **53**, (1961).

Wen, C. Y., and L. H. Chen, "Fluidized Bed Freeboard Phenomena: Entrainment and Elutriation," *AIChE J.*, **28**, 117 (1982).

Wu, R. L., J. Lim, J. Chaouki, and J. R. Grace, "Heat Transfer from a Circulating Fluidized Bed to Membrane Water Wall Surfaces," *AIChE J.*, **33**, 1888 (1987).

Wu, R. L., J. R. Grace, C. J. Lim, and H. Brereton, "Suspension to Surface Heat Transfer in a Circulating Fluidized Bed Combustor," *AIChE J.*, **35**, 1685 (1989).

Yerushalmi, J., N. T. Cankurt, D. Geldart, and B. Liss, "Flow Regimes in Vertical Gas-Solid Contact Systems," *AIChE Symp. Ser.*, **176**, No. 74, 1 (1978).

Yoshida, K., D. Kunii, and O. Levenspiel, "Heat Transfer Mechanism between Wall Surface and Fluidized Bed," *Int. J. Heat Mass Transfer*, **12**, 529 (1969).

Manuscript received June 18, 1990, and revision received June 4, 1991.